Journal Pre-proof

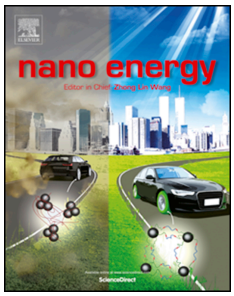

Oxygen-Functionalized Soft Carbon Nanofibers as High-Performance Cathode of K-Ion Hybrid Capacitor

Chenglin Zhang, Yang Xu, Guangyu Du, Yuhan Wu, Yueliang Li, Huaping Zhao, Ute Kaiser, Yong Lei

PII: S2211-2855(20)30218-4

DOI: https://doi.org/10.1016/j.nanoen.2020.104661

Reference: NANOEN 104661

To appear in: *Nano Energy*

Received Date: 4 November 2019

Revised Date: 14 February 2020

Accepted Date: 28 February 2020

Please cite this article as: C. Zhang, Y. Xu, G. Du, Y. Wu, Y. Li, H. Zhao, U. Kaiser, Y. Lei, Oxygen-Functionalized Soft Carbon Nanofibers as High-Performance Cathode of K-Ion Hybrid Capacitor, *Nano Energy*, https://doi.org/10.1016/j.nanoen.2020.104661.

Credit Author Statement

C.L.Z and Y. X. contributed equally to this work. Conceptualization, C.L.Z., Y.X., and Y.L.; Methodology, C.L.Z.; Investigation, C.L.Z., G.Y.D., Y.H.W., Y.G.F, Y.L.L., and U.K.; Writing – Original Draft, C.L.Z. Writing – Review & Editing Y.L.; Funding Acquisition, Y.L.; Resources, H.P.Z., and M.Z.; Supervision, Y.L.

Graphitic Abstract

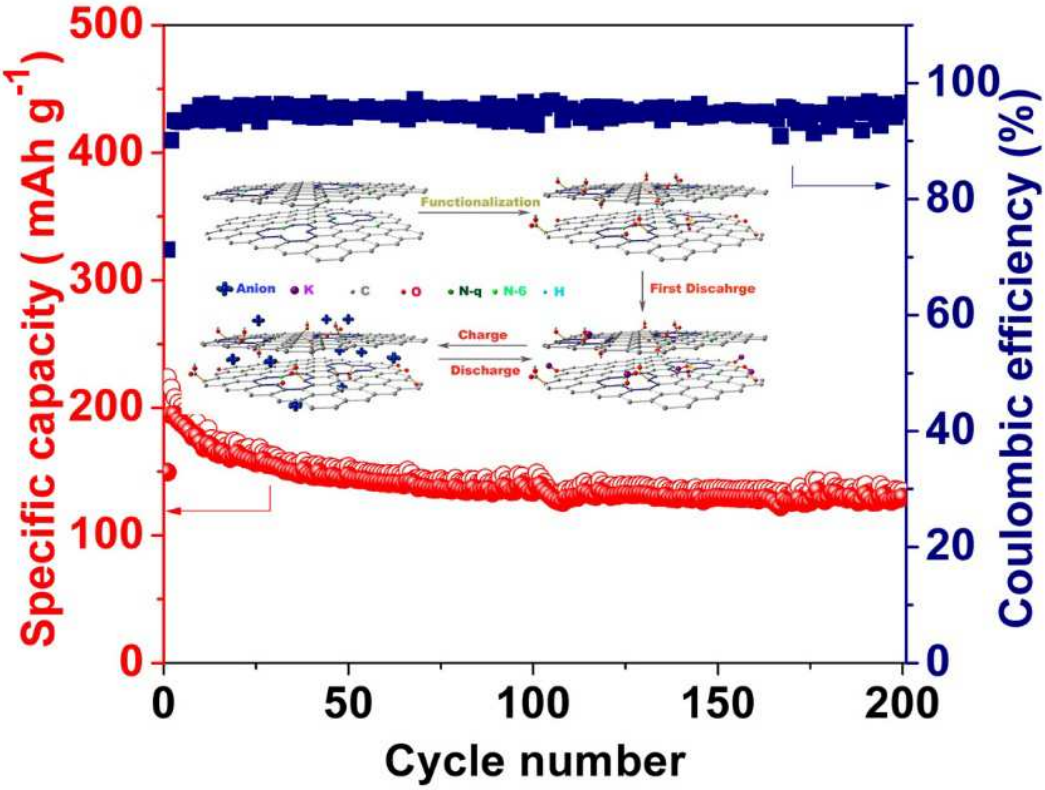

Oxygen-Functionalized Soft Carbon Nanofibers as High-Performance Cathode of K-Ion Hybrid Capacitor

Chenglin Zhang[1], Yang Xu[1], Guangyu Du[2], Yuhan Wu[1], Yueliang Li[3], Huaping Zhao[1], Ute Kaiser[3], Yong Lei[1]*

[1]Institute für Physik & IMN MacroNano (ZIK), Technische Universität Ilmenau, Ilmenau 98693, Germany.

[2]School of Environmental and Chemical Engineering, Shanghai University, Shanghai 200444, China.

[3]Central Facility for Electron Microscopy, Electron Microscopy Group of Materials Science, Ulm University, Ulm 89081, Germany.

Corresponding Author: yong.lei@tu-ilmenau.de

Abstract: Facing the calling for the new generation of large-scale energy storage systems that are sustainably low cost based on earth-abundant and renewable elements, the K-ion hybrid capacitor (KIHC) constructed with both carbonaceous cathode and anode will be one of the best choices. By using oxygen-functionalized engineering, we first obtained oxygen-containing soft carbon nanofibers (ONC) cathodes which delivered a high reversible capacity of 130 mAh g^{-1} over 200 cycles at a current density of 50 mA g^{-1} within a high voltage window. Even at 5.0 A g^{-1}, a practical capacity of 68 mAh g^{-1} maintained. The surface-controlled reaction domination instead of diffusion-controlled reaction domination was proposed to harvest high capacitance performance. This storage model effectively overcomes the sluggish properties of storing large-sized K-ions by a diffusion-controlled reaction in conventional cathodes in K-ion batteries (KIBs).

The rational design of oxygen functionalization towards approaching more and stable active sites was highlighted. Moreover, a renewable and low-cost full KIHC was configurated by carbonaceous cathode and anode deriving from a single carbon source.

Keywords: Energy storage; K-ion hybrid capacitor; Oxygen-functionalized engineering; Carbon nanofibers

Graphical Abstract:

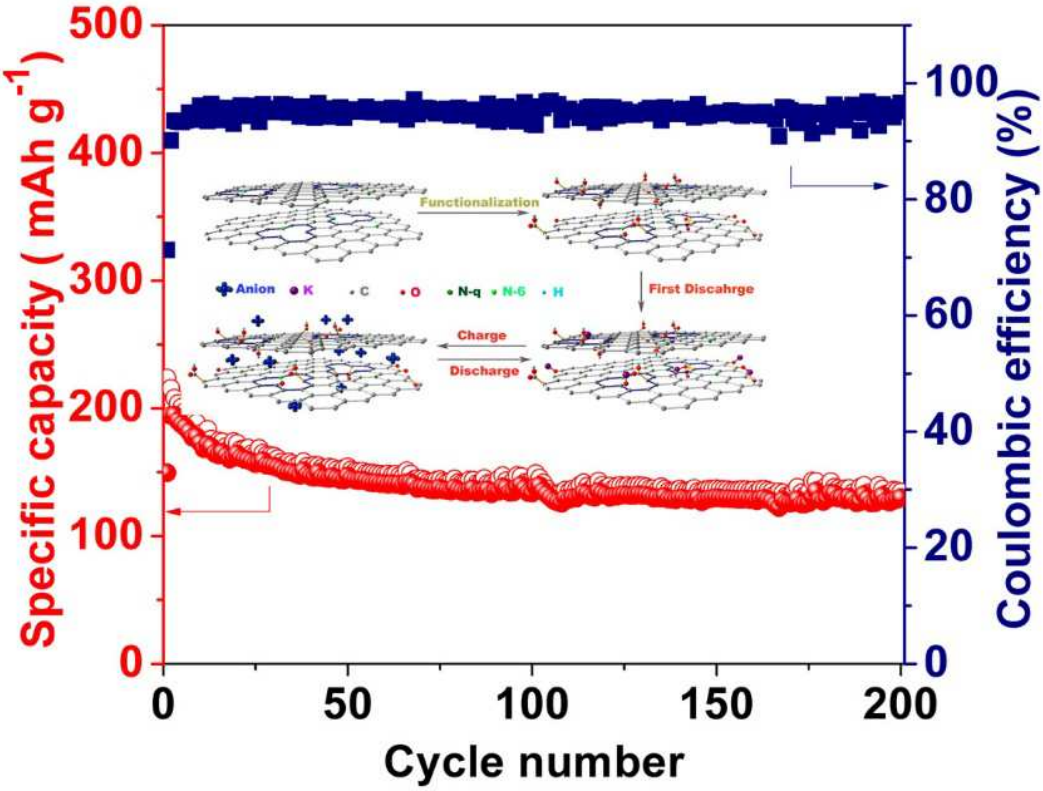

1. Introduction

The collection of renewable energy sources with an intermittent nature demands new sustainable energy storage technologies. Among various electrochemical energy storage systems, Li-ion batteries (LIBs) have certainly been a contender, but they suffer from a critical challenge

of the rapidly increasing cost due to the scarcity and maldistribution of the lithium resources. Recently, KIBs have attracted much attention as a potential alternative of LIBs owing to the abundant reserves of K resources (almost 1000 times larger than Li) and similar electrochemical energy storage mechanism to LIBs. [1] Furthermore, K has a close electrochemical potential comparing to Li (-2.93 V for K/K^+ and -3.04 V for Li/Li^+, vs. standard hydrogen electrode), which makes KIBs more competitive than Na-ion batteries in terms of working voltage and energy density. [2-4]

The proven fact that K-ion, unlike Na-ion, can intercalate into graphite in organic electrolytes has driven a large body of study on KIBs. It has resulted in greatly developed anode materials during the past few years,[3] and delivered anodes with large capacities and great rate capability that certainly benefits fast-charge and -discharge property. Carbon materials exhibited reversible capacities of over 150 mAh g^{-1} at a current density of 1.0 A g^{-1}. [5-7] Organic materials such as dipotassium terephthalate could maintain a capacity of 202 mAh g^{-1} at the same current density. [8] However, the development of cathodes is unbalanced, and their rate capability is unsatisfactory, which imposes a great challenge of full-cell assembly due to the lack of the matched rate with anodes. [9-16] Conventional intercalation-type cathode materials suffer from slow K-ion diffusion because of the larger size of the ions (K-ion: 1.38Å > Na-ion:1.02 Å > Li-ion: 0.76 Å), and the resulting kinetic limitation often leads to a high coefficient of volume expansion and difficulties of fast K-ion diffusion at high charging and discharging rates. So far, cathode materials of KIBs have rarely exhibited a practical capacity at a current density of 1.0 A g^{-1}. Therefore, there exists an immediate need to improve the rate capability of K-ion storage.

As a supplementary of KIBs, potassium ion capacitors (KICs) would be appealing to serve as a promising alternative to lithium-ion capacitors (LICs). So far, a few works have been reported

for the KIC research, such as soft carbon,[17] $Ca_{0.5}Ti_2(PO_4)_3$@C, [18] $K_2Ti_6O_{13}$, [19] organic K_2TP, [20] Nitrogen-doped MoSe/Graphene, [21] Oxygen-rich carbon nanosheets, [22] porous MXenes, [23] CoP nanorods, [24] Onion-like carbon, [25] $FeSe_2$/N-C, [26] $K_{0.45}Mn_{0.5}Co_{0.5}O_2$, [27] 3D nitrogen-doped framework carbon, [28] and AC-HC. [29] However, most of them focus on developing anode materials for KICs, active carbons are commonly employed as the cathodes. Therefore, from our point of view, searching for new cathode materials of KICs especially for low-cost carbon cathode materials is extremely urgent and present a timely issue for the KIC research. Moreover, the mechanism investigation of K-ion adsorption on carbon cathode is rarely reported, and hence the understanding of the K-ion adsorption of the oxygen functional groups in carbon materials is crucial for KIC cathode research. Bearing in mind that K-ion diffusion in solid is the limiting factor to achieve high rate capability, we propose a KIHC system to storage K ions, which performs surface-controlled reaction as a dominating contributor that enables fast-charge and -discharge property of cathode materials. Our proposal is inspired by the carbonyl-containing organic electrodes, [30-31] based on which the redox reaction between the oxygen functional groups and K-ions, i.e., $-C=O + e + K^+ \leftrightarrow -C-O-K$, is expected to realize reversible K-ion storage in carbon materials. The proposal possesses two advantages to achieve high rate capability of K. First, the oxygen functional groups could be bonded on the surface of the carbons, and thus surface-contributed capacity could be obtained by the aforementioned reaction. Second, the incorporation of the oxygen functional groups could expand the interlayer space of the carbons, and thus an improved K-ion diffusion to access the groups could be expected. The two advantages can ensure the utilization of surface-controlled reaction to a maximum extent, thereby reducing the heavy reliance on the K-ion diffusion in solids.

Based on our proposal, it is critical to have the ease of modifying the surface of the carbons

with a large amount of oxygen functional groups. The edges of graphene layers in carbons tend to show a higher chemical reactivity than the graphitic bases (the aromatic rings), and thus work as redox-active sites. [32] Creating more edges of graphene layers is expected to increase the ease of surface functionalization. Our previous work of KIB anodes has demonstrated that nitrogen-doping can effectively create defects within the graphene layers of carbons, which induces more edges of the layers. [33] It encourages us to use nitrogen-doped soft carbons as a starting material to perform the oxygen functionalization. Considering the low-cost and material sustainability, it also forms a perfect base to construct all-carbon KIHC consisting of oxygen functionalized carbons as cathodes and nitrogen-doped carbons as anodes.

Herein, by modifying three-dimensional (3D) network of nitrogen-doped carbons (NC) using a solution of mixed acids, we fabricated oxygen-functionalized carbon nanofibers (ONC) as KIHC cathodes. The oxygen-containing functional groups are chemically bonded at the graphene edges, resulting in reversible storage of K-ions in a high voltage window through surface faradic reaction. The ONC electrode exhibited a reversible capacity of 130 mAh g^{-1} at a current density of 50 mA g^{-1} over 200 cycles in a voltage window of 1.2-4.2 V. Even at 2 and 5.0 A g^{-1}, it still delivered capacities of 72 and 68 mAh g^{-1}, respectively. We studied the electrochemical mechanism and revealed that the large reversible capacity and excellent rate capability are owing to a large surface-controlled capacity which was mainly realized by the faradic reaction between K^+ and C=O. The optimal engineering of the oxygen functionalization suggests a soft carbon precursor with suitable graphitization and defects would be a better choice for obtaining stable and oxygen-rich carbon in strong acid. Furthermore, we presented a cost-effective and “green” full KIHC based on the ONC cathode and NC anode. It delivered a capacity of 84 mAh g^{-1} at a current density of 100 mA g^{-1} over 50 cycles. Even at 1.0 A g^{-1}, it still delivered a capacity of 43

mAh g^{-1}. Such behaviors outperform the performances of many other full-carbon K-ion storage systems. [34-37] This work manipulates one carbon material into both cathode and anode materials and paves a new approach for obtaining the KIHC cathode materials and renewable commercial batteries.

2. Material and methods

2.1 Nitrogen-doped carbon nanofibers (NC) preparation

The nitrogen-doped carbon nanofibers were fabricated by a facile method reported in our previous work. [33] In a typical process, 0.8 g cetrimonium bromide (CTAB, $(C_{16}H_{33})$-$N(CH_3)_3Br$) was dissolved in 240 ml of 1 mol L^{-1} hydrochloric acid solution. After a transparent solution formed, 1.2 g Ammonium persulfate (APS, $(NH_4)_2S_2O_8$) was then added into the above solution. A homogeneous white suspension formed under magnetic stirring for 30 min. 1.6 ml pyrrole monomer was then dropwise added into the white suspension and the polymerization was carried out in the ice bath (0-3□) for 3 hr under strongly stirring. Subsequently, a black precipitate (PPy precursor) was collected by filtration and washed with deionized water until the filtrate became colorless. The PPy precursor was dried at 80 □ in a vacuum oven for 24 hr and NC was obtained by annealing it at 1100 □ in N_2 atmosphere with a ramp rate of 5 □ min^{-1} for 2 hr.

2.2. Oxygen-functionalized carbon nanofibers (ONC) preparation

In brief, 20 ml mixed strong acids solution of H_2SO4/HNO_3 (vol 3/1, 96% and 70%, respectively) was fabricated in a 50 ml round-bottom flask. 150 mg as prepared NC was then put in the acid solution and kept the flask in the oil bath at 50 □ under mild magnetic stirring for 1hr. After diluting the mixed solution, the ONC was washed until the solution became neutral and dried in a vacuum oven at 80 □ for 24 hr before use. The comparison samples (ONC650, ONC800, and ONC950) were obtained through annealing PPy precursor at 650, 800, and 950 □

respectively, then conducting the oxygen functionalization.

2.3 Materials characterization

The SEM was performed on a Hitachi 434 S4800 to observe the morphology of the samples. TEM and elemental mapping were performed on a JEOL JEM-435 2100F to analyze the construction of the samples. The crystal features of the samples were identified with the XRD pattern using an 18 KW D/MAX2500V PC diffractometer at a scan rate of 2° min^{-1}. The X-ray photoelectron spectra analysis was acquired with a Thermo 436 SCIENTIFIC ESCALAB 250Xi using an Al Kα (hυ = 1486.8 eV) as the excitation source. The Raman spectra analysis was carried out using an inVia Raman microscope with He-Ne laser (532 nm). FTIR spectra were performed on an AVATAR 370. A Quantachrome autosorb IQ automated gas sorption analyzer was employed to conduct the BET measurement analysis, the size and distribution of the pores (mesopores and macropores) on the samples' surface then can be obtained.

2.4. Electrochemical measurements

The electrodes were prepared by mixing 80 wt% as-synthesized carbon materials, 10 wt% Super P, and 10 wt% polyvinylidene fluoride (PVDF). Then, the slurry was coated on a copper foil using the doctorblade that controlled the active materials loading amounts to around 2.0 mg cm^{-2} and put the foils in a vacuum oven at 110 □ for 12 hr. The electrochemical properties were measured using the coin-cell configuration (CR 2032) which were assembled in N_2-filled glove-box. The electrolyte of 0.8 M KPF_6 in ethylene carbonate and propylene carbonate (vol EC/PC = 1/1) also was prepared in the glove-box. The separator was a glass microfiber filter (Whatman, Grade GF/B). The K foil was used as the counter electrode for the half-cell. CV tests were carried out with various scan rates on a VSP electrochemical workstation (Bio-Logic, France). Galvanostatic charge/discharge tests were performed on a Land CT 2001A 449 battery testing

system (Land, China) under different current densities at ambient temperature. For the full cell, the NC without functionalization was used as the anode electrode. The cathode limited configuration was used to prepare the anode and cathode films. The specific capacity of the full cell was calculated based on the weight of the cathode. The mass-loading ratio is around 1.3.

3. Results and discussions

3.1 Synthesis and characterization of ONC

The ONC nanofibers were obtained by a mixed-acid treatment of the NC nanofibers. Figure 1A and Figure S1 show the scanning electron microscope (SEM) images of ONC with different magnifications, demonstrating a 3D network that is consisting of nanofibers with an average diameter of ~80 nm. ONC faithfully inherited the morphology of NC (Figure S2), suggesting that it has a minimal effect on the morphology of the carbons to functionalize them with the oxygen groups. Figure 1B shows the transmission electron microscopy (TEM) image of ONC reveals the hollow inner of the ONC nanofibers. The thickness of the sidewall is ~25 nm, forming tubes with an inner diameter of 30-40 nm. Such a 3D network assembled by the interconnected hollow nanofibers makes surface-reaction and electron transport effective. High-resolution TEM (HRTEM) image (Figure 1C) shows ONC consists of many micro-areas where short-range ordered graphene layers can be found. The micro-areas are separated by the micropores that can be considered as carbon defects and create graphene edges on which the redox-active oxygen groups can be functionalized. [32] The similarity of the macro- and micro-structures between ONC and NC proves the rationale of choosing NC as the starting material (HRTEM of NC1100, Figure S3). [33] As shown in the element mapping images (Figures 1D-G), carbon and oxygen distribute evenly over the entire nanofiber, further confirming the successful functionalization of the oxygen groups. The incorporation of oxygen also reduces the amount of nitrogen compared

with NC.

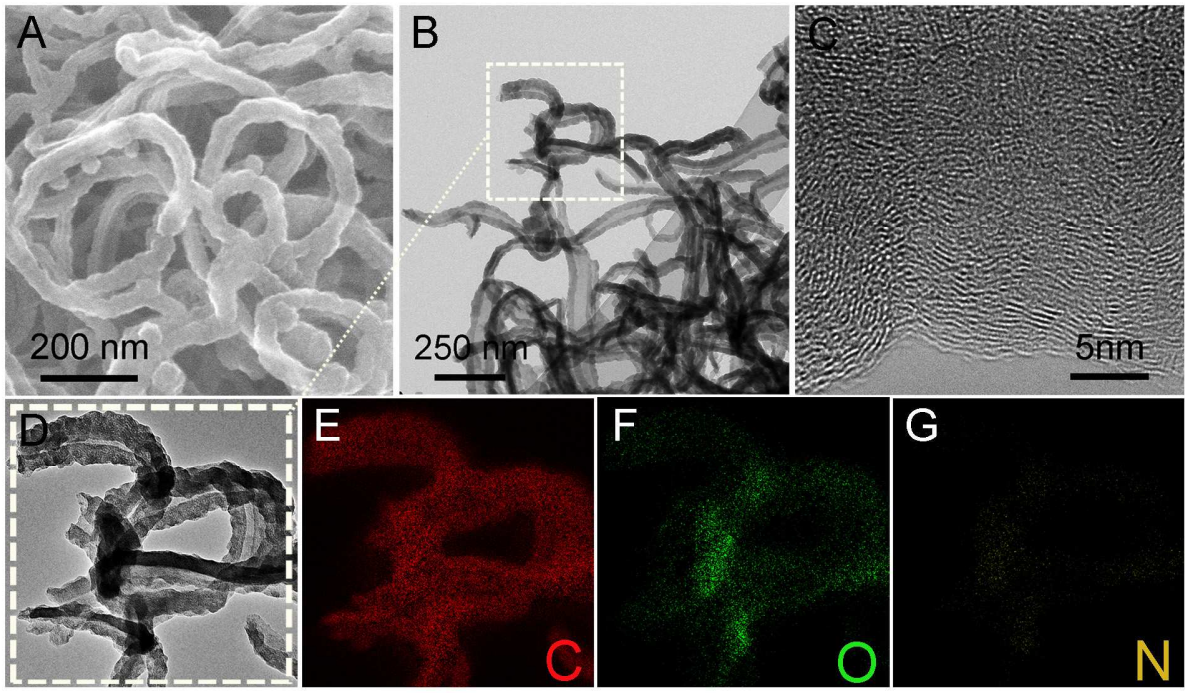

Figure 1. Structure characterization of ONC by electron microscopes. (A) SEM image. (B) TEM image. (C) HRTEM image. (D-G) Images of element mapping of C, N, O.

The structure of ONC and NC were analyzed by X-ray diffraction (XRD), Raman spectroscopy, Fourier Transform Infrared (FTIR) spectroscopy, X-ray photoelectron spectroscopy (XPS) and Brunauer-Emmett-Teller (BET). The XRD patterns in Figure 2A show both ONC and NC possess two peaks at around 25°and 43°, which can be indexed to (002) and (101) planes of a disordered carbon, respectively. Upon functionalization, the oxygen functional groups modified at various locations on both sides of graphene layers can cause distortion of the inter-planar space, resulting in the widening of the diffraction peaks. The (002) peak of ONC shifts from 26° to 24°, indicating the expansion of the inter-planar spacing caused by the oxygen functional groups. [38] The Raman spectra of ONC and NC (Figure 2B) both exhibit broad disorder-induced D-band

(1353 cm^{-1}) and in-plane vibration G-band (1579 cm^{-1}). The value of I_G/I_D can be used to verify the graphitic ordering of amorphous carbon materials, [39] where I_G and I_D are obtained from the absolute heights of the peaks. The calculated value of I_G/I_D decreases from 1.04 for NC to 0.94 for ONC after functionalization, indicating a higher disordering degree of ONC and agreeing with the XRD results. The FTIR spectrum of the NC in Figure 2C exhibits overlapping bands in 1500-1600 cm^{-1} range corresponding to the C-sp^2 hybridization, suggesting the presence of considerable amounts of aromatic domains in NC sample. In the spectrum of ONC, the overlapping bands located in 750-1500 cm^{-1} can be assigned to the C-O, C-O-C, and O-H vibrations. The peak of the ONC spectrum between 1600 and1700 cm^{-1} corresponding to the COOH and C=O mode becomes much sharper, and the presence of a peak around 3400 cm^{-1} suggests the existence of C-OH mode. [40-41] According to the comparison of different oxygen bonds, the spectra confirm that oxygen-containing groups have been chemically bonded with the edges of the carbon rings. The XPS survey spectra in Figure 2D show a sharp increase of the O1s peak intensity in ONC, once again demonstrating that the oxygen functionalization process has been realized. The content of oxygen increased from 1.1% to 19.8% meanwhile the composition of the C=C bond decreased from 75.8% to 69.9%, which results from the harsh oxidation and destruction of the C-sp^2 aromatic structure of graphitic edges in a strongly oxidizing solution. The contents of C=O groups, C-O-C/C-OH groups, and COOH groups are about 36%, 45%, and 19% respectively. It suggests that both C=O groups and C-O-C/C-OH groups play a major role in the K-ion storage (Figure S4A). A slight reduction in nitrogen content may be due to acid corrosion and the addition of oxygen atoms. The ONC contains only N-6 and N-Q (Figure S4B), and the N content in ONC is sufficiently low (nearly 2%) that it is not expected to meaningfully contribute to the charge storage capacity. Figure 2E displays close observation of the C1s XPS spectra of

ONC and NC. The peaks can be fitted to five components located at 284.7, 285.6, 286.7, 288.2 and 290.1 eV, corresponding to the sp^2 C(C=C), sp^3 C (C-C, C-O, C-N), C=O, COOH, and N-C=O groups, respectively. [42-43] It is noted that the relative content of oxygen functional groups (C=O and COOH) increased in ONC in comparison with NC. The hysteresis loop of nitrogen absorption/desorption isotherms in Figure 2F demonstrates that ONC possesses the characteristic of the H3-type adsorbent feature, meaning both macro- and mesopores exist in the carbon. The BET surface area was estimated to be 123.6 m^2 g^{-1}. The pore size distribution analyses of ONC (inset of Figure 2F) also confirms the existence of macro- and meso-pores, which corresponds to the porous structure between the short-range graphene layers and the inner diameter of the hollow fibers, respectively, agreeing *w*ith the results of TEM and SEM characterizations.

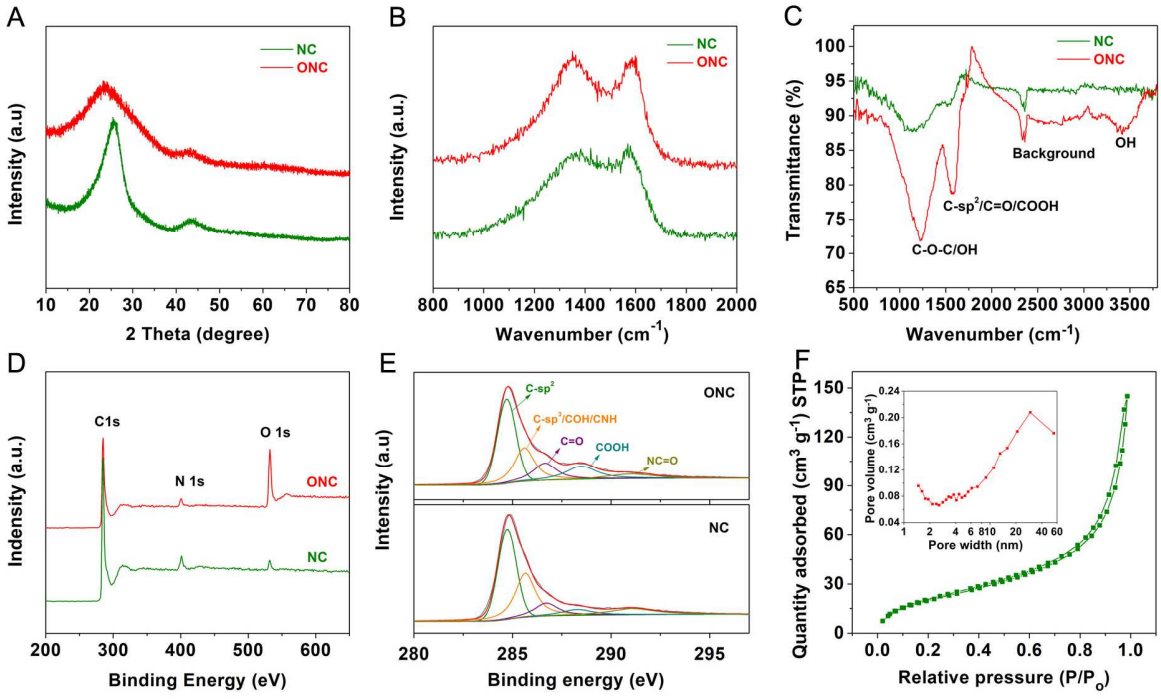

Figure 2. Structure characterizations of ONC and NC by spectroscopes. (A) XRD patterns. (B) Raman spectra. (C) FTIR spectra. (D-E) XPS survey spectra and C 1s core level of XPS high-resolution spectra. (F) Nitrogen adsorption/desorption isotherms (inset).

3.2 Investigation of electrochemical performance of ONC

The electrochemical behavior of ONC was investigated in a voltage window of 1.2-4.2 V in half-cells. As shown in Figure 3A, the cyclic voltammetry (CV) curves at a scan rate of 0.2 mV s^{-1} display a quasi-rectangular shape with less defined peaks, indicating the oxygen functional groups of ONC undergo a faradaic reaction which is responsible for electrochemical energy storage at the applied voltage window typically for cathode materials. [42] Figure 3B shows the cycling performance measured at a current density of 50 mA g^{-1}, and the charge-discharge profiles are shown in Figure S5. The profiles display a sloping feature in the applied voltage window, which is consistent with the CV results and signals a surface-controlled charge storage mechanism. ONC delivered initial discharge and charge capacities of 160 and 224 mAh g^{-1}, respectively. The higher capacity of the charging process implies the contribution of anion (PF_6^-) storage to the total capacity. We tested the half-cell in the same voltage window but starting from a charging process (Figure S6). The initial charge capacity of 56 mAh g^{-1} was obtained, which proves the concurrent occurrence of anion storage. Coulombic efficiency (CE) increased to 95% after 10 cycles, demonstrating high reversibility of the charge storage derived from the reduction/oxidation of the oxygen functional groups (will be discussed later). ONC delivered a capacity of 130 mAh g^{-1} after 200 cycles, maintaining 70% of the discharge capacity of the 5th cycle. The obtained long-term capacity is comparable or even higher than those of the conventional KIB cathodes. [9-16] To further confirm that the oxygen functional groups are responsible for the charge storage, we tested NC in a half-cell with the same condition. As shown in Figure S7 and S8, a low capacity of ~40 mAh g^{-1} was observed, and the capacity contribution from the voltage above 2.0 V is about 30% of that in ONC due to the lack of charge storage sites in NC. Rate performance at various current densities was presented in Figure 3C. ONC delivered

reversible capacities of 194, 148, 123, 100, 85, 72, and 68 mAh g^{-1} at the current densities of 0.05, 0.1, 0.2, 0.5, 1.0, 2.0, and 5.0 A g^{-1}. The capacity recovered to 155 mAh g^{-1} when the current density was reduced back to 0.05 A g^{-1}. Moreover, we further tested for 50 additional cycles, and it exhibited a stable reversible capacity of 131 mAh g^{-1}. Stable and well-reproducible charge-discharge profiles were observed at all testing current densities (Figure 3D), and almost no polarization between charging and discharging can be found, once again demonstrating the high reversibility and facile charge transport of the oxygen functional groups enabled charge storage. Moreover, we investigated the ONC electrode at high current densities of 1.0 A g^{-1} and 2.0 A g^{-1}. The capacity can remain 65 mAh g^{-1} after 1000 cycles and 48 mAh g^{-1} after 3000 cycles respectively (Figure 3E). As previously pointed out, there have been very limited reports of conventional KIB cathode materials that exhibit a practical capacity at 1.0 A g^{-1}. [44-47] The presented rate capability in our work not only shows a practical capacity at such a current density but also maintains among high capacities at the current densities well beyond 1.0 A g^{-1}.

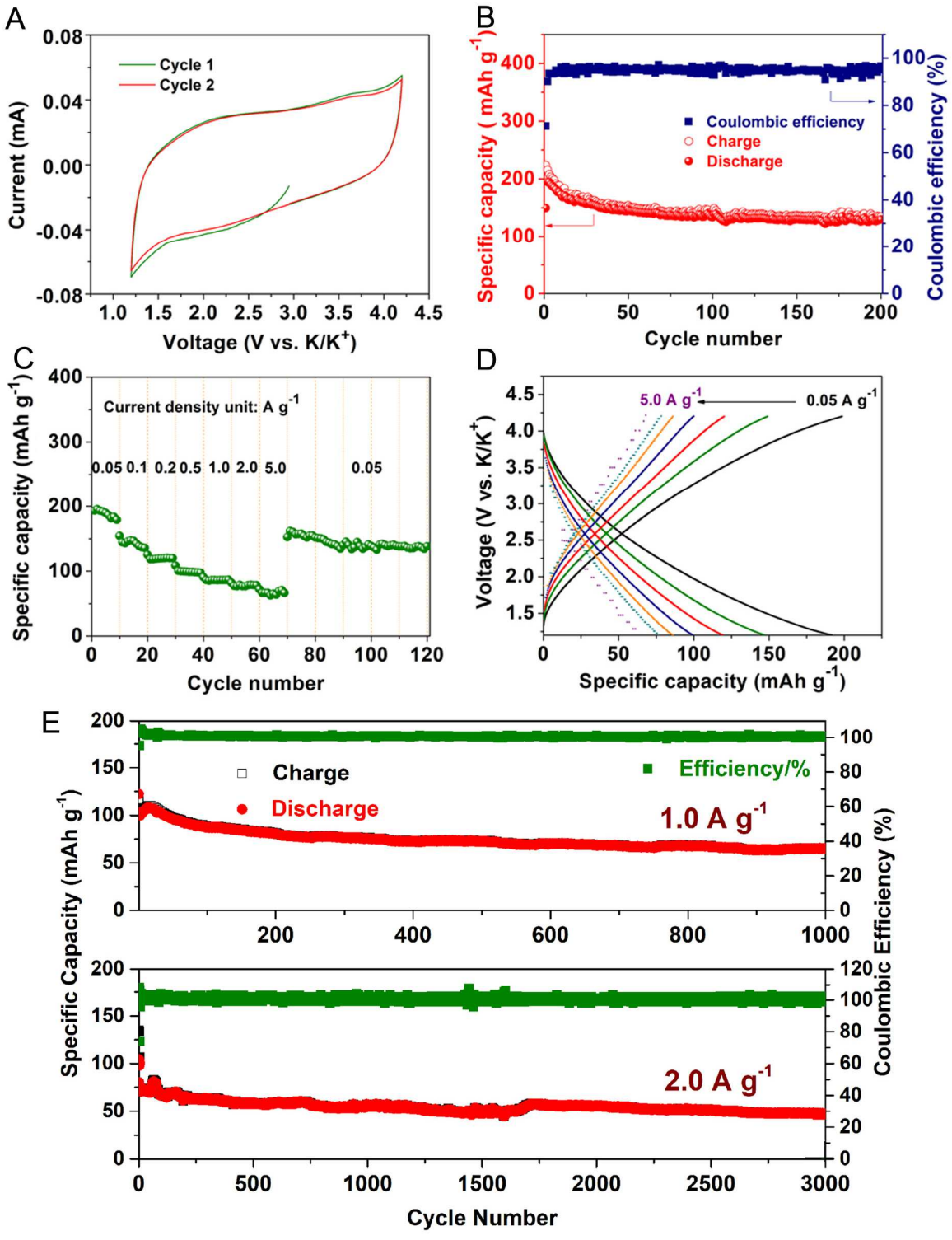

Figure 3. Electrochemical performance of ONC in a half-cell configuration. (A) CV curves at the scan rate of 0.2 mV s^{-1}. (B) Cycling performance at the current density of 0.05 A g^{-1}. (C) Rate

performance. (D) Profiles with rates ranges from 0.05 to 5.0 A g^{-1}. (E) Cycling performance at high current densities of 1.0 A g^{-1} and 2.0 A g^{-1}.

3.3 Undergoing electrochemistry of ONC

To reveal the charge storage mechanism, we conducted the XPS measurement on the ONC electrodes at different charge and discharge states, and the results are shown in Figure 4. The O 1s spectra can be fitted to three components of C=O, -OH/-O-, and COOH at the bonding energies of 530.2, 532, and 533 eV, respectively (Figure 4A). The relative intensity of C=O to -OH/-O- decreases after first discharging process and increases after the subsequent charging process. It is in accordance with the reaction of -C=O - e ⇌ -C-O-, where C=O double bond is reduced to C-O single bond upon an electron released, while the opposite process occurs after capturing an electron. We notice that the relative intensity of C=O does not fully recover after the first charging process, presumably resulting from the competition between reversible and irreversible oxidation of the functional groups of -C-O- in ONC, which was observed in previous work. [48] Nevertheless, a significant decrease of the relative intensity after the second discharging process suggests a reversible reduction of C=O and thereby the reversible redox reaction can be confirmed. The changing trend of the C 1s components is in a good agreement with the O 1s components (Figure S9), where the reversible change of relative intensity of C=O to C-O can be clearly identified. The results of the K 2p spectra shown in Figure 4B provide additional support to the presented charge storage mechanism of -C=O + K^+ - e ⇌ -C-O-K. The intensity of the peaks increases/decreases after each discharging/charging process, indicating the storage/release of K-ions by/from the oxygen functional groups, which is also in a good agreement with the results of the O 1s and C 1s spectra. As we mentioned in the last section, anion storage also contributes to the overall charge storage. Since PF_6^- carries negative charge,

the change of its amount should be opposite to that of K-ion. This is exactly what we observed in the F and P spectra (Figure 4C), where the intensities of the F 1s, P 1s, and P 2p peaks all increase after charging process and decrease after the subsequent discharging process. [49] However, the low absolute intensity and the relatively smaller change comparing with the O and K peaks undoubtedly suggest that the K-ion storage by the oxygen functional groups is the major contributor to the overall capacity. On the basis of the above analysis, the charge storage mechanism is illustrated in Figure 4D. The functionalization of the oxygen groups preferentially occurs at the defect sites of graphene layers induced by the nitrogen doping. C=O groups are reduced to C-O upon the uptake of K-ions during the first discharge process, and reversible reduction/oxidization of C=O and storage/release of PF_6^- take place during the subsequent cycles. Furthermore, the types and bonding environment of the oxygen functional groups could be the major influence factor of the material stability in this work. As we know, the reversible reaction of oxygen-containing functional groups to potassium ions is mainly because the electrons of the C=O bond can be delocalized to other C=C bonds. [**R5**] The sp^2 hybridization of C=C bonds in carbon molecules rings is weaker than the sp^2 hybridization of C=C bonds in organic aromatic rings because of the existence of π^* bonds. Therefore, the reversibility and stability of the oxygen functional groups depend on whether the electrons at the active sites can delocalize and the sp2 hybrid strength of the carbon ring where the oxygen function is located. In our work, the ONC possesses three different kinds of oxygen-containing functional groups (***Figure S11***), type A possesses the highest chance for the electron delocalization of C=O bonds. The weaker type B and type C shall be playing a major role in the degradation of material properties. It can be speculated that the ion diffusion in the carbon layer after long cycles weakens the sp2 hybridization of carbon, which further reduces the activity of weak type B and type C. In addition,

the charge and discharge plateaus for carboxylic groups (Type B) of the organic aromatic compounds are generally lower than 1.0 V, they are mainly used for K-ion storage of the anode materials. [**R8-R10**] Therefore, the carboxylic groups may not store potassium ions at high voltages in oxygen-functionalized carbon materials. The relative intensity of the carboxylic functional groups in Figure 4A has hardly changed during the charging and discharging process, which can support that.

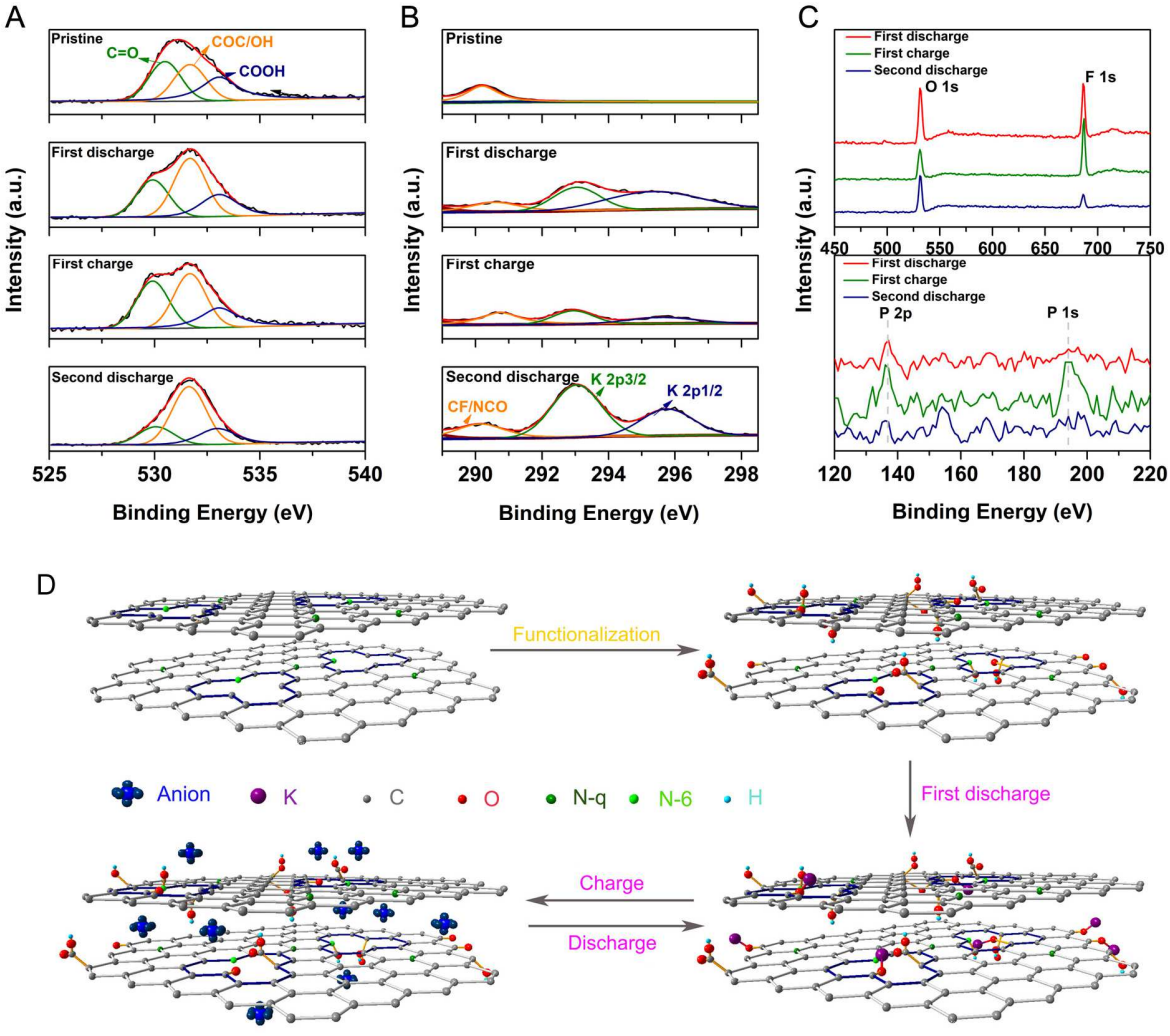

Figure 4. Electrochemical mechanism study with ex-situ XPS spectroscopes of ONC. (A) O 1s core level of XPS spectra at different charge and discharge states. (B) K 2p core level of XPS

spectra screenshot from the figure of C 1s core level of XPS spectra. (C) F 1s core level of XPS spectra (upper), P 1s and P 2p core level of XPS spectra (lower). (D) Schematic illustration of charge and discharge processes of K-ions and anions in half cell.

3.4 Analysis of the kinetics of K-ion storage

To further study the kinetics of the ONC electrodes, we investigated the CV curves at scan rates of 0.1 to 5.0 mV s^{-1} (in Figure 5A). The peak current obeys a power-law relationship with scan rate, which can be used to reveal the charge storage process according to the following equation:

$$i = av^b$$

where *i*-value is peak current, *v*-value is scan rate, *a* and *b* are adjustable values. Whereas a *b*-value of 0.5 corresponds to an ideal intercalation Faradaic reaction process and a *b*-value of 1 corresponds to an ideal surface faradaic reaction controlling. [54] Figure 5B shows a good linear relationship based on the cathodic peak current and the *b*-value is calculated to be 0.83, suggesting a surface dominated process. The surface process contribution can be further quantitatively estimated according to following equation.

$$Q = Q_\infty + \text{const}\ (1/v)^{-1/2}$$

where *Q*-value is capacity, *v*-value is scan rate. Q_∞ is a constant value that is assigned to the ideal storage capacity at infinity rate. [54-55] In a plot of *Q* versus $v^{-1/2}$, the relationship between discharge capacity and scan rate can be established, and the regions that are linear represent capacity limited by semi-infinite linear diffusion-controlling whereas surface-controlled contributions are independent. As shown in Figure 5C, the ideal storage capacity by surface-controlling is estimated to 0.087 mAh. The fast charge/discharge kinetic at high rates (> 1.0 mV s^{-1}) is dominated by a surface-controlled reaction. In addition, the level of the surface-control

reaction contribution also was determined according to the relation of current density, *i*, with the combination of capacitor-like index, $k_1\nu$, and diffusion-controlled index, $k_2\nu^{1/2}$. [7, 12, 33] At the scan rate of 1.0 mV s^{-1}, the surface-controlled contribution is 51.6% (Figure 5D). Similar to supercapacitors, the main factor for high rate charge/discharge is the transfer of ions and electrons to the surface of nanofibers rather than the conventional bulk diffusion. This is unsurprising since N–dopant in carbon precursor could induce more defects and edges of graphene layers, which results in more bonding with oxygen-containing functional groups as a surface functionalization.

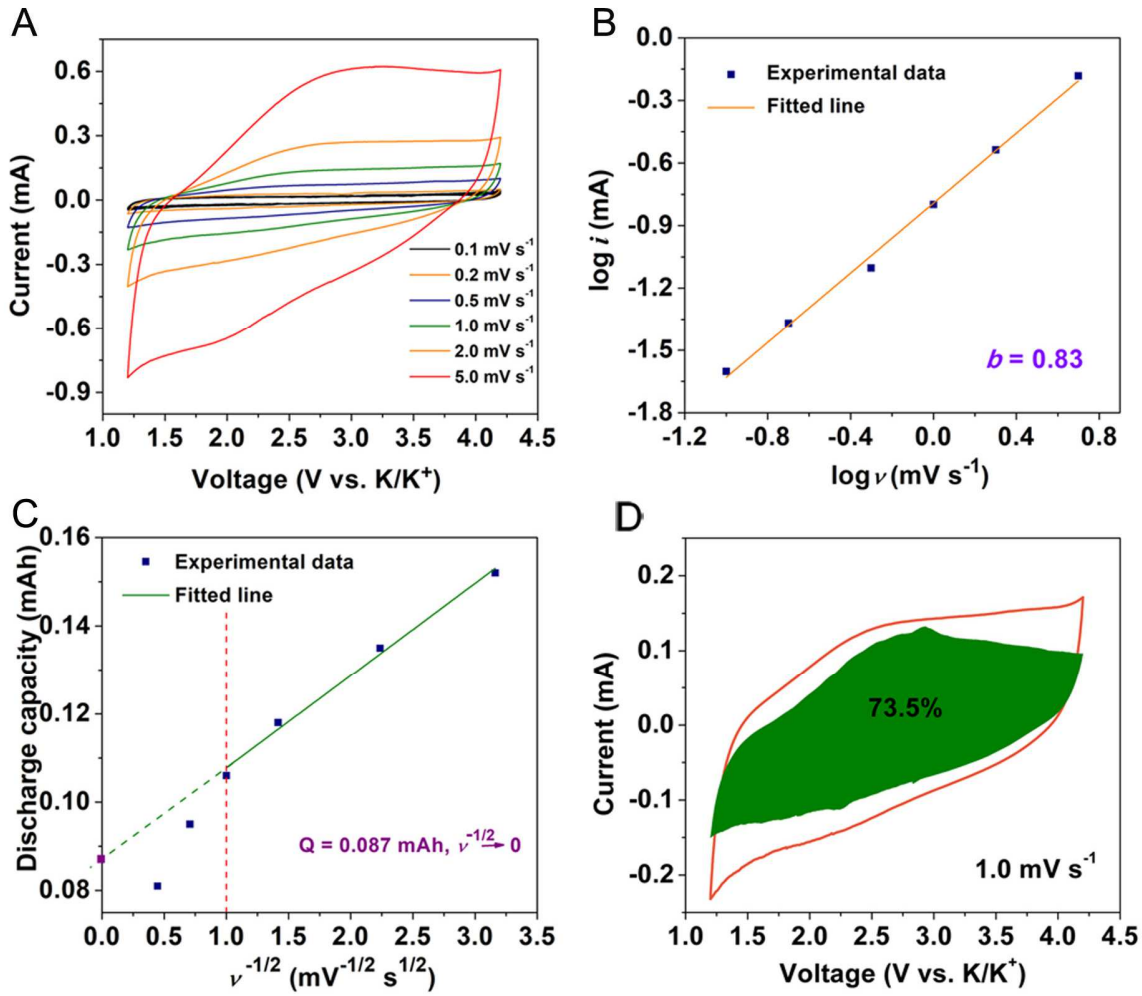

Figure 5. Quantitative analysis and illustration of K-storage process in ONC. (A) CV curves at various scan rates of 0.1 mV s^{-1} to 5.0 mV s^{-1}. (B) b value determination from anodic peaks currents. (C) Separation of diffusion-controlled capacity from capacitive-controlled capacity. (D) The contribution of surface reaction at 1.0 mV s^{-1}.

3.5 Discussion of optimal engineering of oxygen functionalization

The oxygen-containing groups and the stability of the surface reaction are two factors to achieve high capacity and cycling behavior. Those are relevant to the contents of oxygen-containing groups at the graphene edges and their graphitic environment (the aromatic rings). Therefore, increasing both graphene edges and degree of graphitization which create much stable redox-active sites are necessary. However, they are competing with each other. In principle, during the degree of graphitization increase, graphene edges will decrease for carbon materials. In this case, to understand the correlation and further explain the optimal performance of ONC, the control experiments were conducted, the comparisons of the cycling performance in the carbon materials with the different functionalization conditions were carried out as well. All the carbon materials underwent galvanostatic charge/discharge processes at 50 mA g^{-1} within voltage windows of 1.2-4.2 V. The ONC with different functionalized temperatures (40 □, 50□, 60□ and 70□) and operation times (1h, 2h, and 3h) were investigated. As shown in Figure S11, the ONC with the functionalized temperature of 50 □ and the operation time of 1h exhibits a higher capacity and more stable cyclability than the other samples obtained at various conditions. It can be speculated that the oxidation of concentrated H_2SO_4/HNO_3 destroys the graphitization of the carbon material while conducting the functionalization process, reducing the content of sp2 hybridization. Functionalization under the conditions of certain temperature and time ensures that the carbon material has a higher content of the oxygen functional groups while ensuring the redox

reversibility of these functional groups. Additionally, the different kinds of oxygen functionalized carbons with different carbon precursors were fabricated. As shown in Figure S12, the ONC with a higher degree of graphitization possesses the greater stability (capacity retention after 100 cycles: 69% for ONC1100; 63% for OCNT; 59% for NC800; 29% for OAC). Moreover, the ONC possesses a better rate capability compared to other analogs. CNT is a graphitic carbon that possesses the highest degree of graphitization and lowest content of defects, it exhibits low capacity but excellent capacity retention. AC is a hard carbon that possesses a relatively low degree of graphitization and high content of defects, it exhibits high capacity but worse capacity retention. Overall, a soft carbon with both lots of defects and a high degree of graphitization which could be a better precursor to obtain an oxygen functionalized carbon for the ion adsorption. Moreover, the K-ion capabilities of the different NC materials of which possess different species of nitrogen defects are also different. The defects in the precursors of NC1100, NC950 and NC800 mainly are the N-6, N-Q which exist in carbon planes through sp^2 hybridization, while that in NC650 mainly are the N-5 which exist in carbon planes through sp^3 hybridization. ONC cathodes possess approximate initial discharge capacities while initial charge capacity shows an obvious difference, the ONC with higher sp^2 hybridization displayed much better reversibility and cyclability. We speculate that the N-6 and N-Q with the sp^2 hybridization give extra electrons delocalization around the N, enhancing the aromaticity of carbon planes, especially the carbon defects. The stronger aromaticity of carbon layers can enhance much delocalization of the electron in carbonyl groups, which might endow much higher stability of ONC at a higher temperature.

3.6 Full-carbon K-ion hybrid capacitor

To demonstrate the potential application of the presented ONC, we paired it with NC to

construct a full-carbon KIHC. The rationale behind it is based on the high working voltage and rate capability of ONC and the low working voltage of NC reported in our previous work (Figure S13). [33 20] Prior to the full-cell assembly, NC was activated by cycling in a half-cell at 50 mA g^{-1} for 10 cycles. As shown in Figure 6A, during charge and discharge, both K-ions and anions can be reversibly stored in ONC, while NC reversibly stores only K-ions. The first charge and second discharge profiles of the full-cell and half-cells are shown in Figure 6B and S14, respectively. The full-cell displays a sloping profile in the voltage window of 0.5-3 V at a current density of 0.1 A g^{-1}, which is related to the similar feature of the ONC half-cell (Figure S5). The charge and discharge capacities are 163 and 100 mAh g^{-1}, respectively, giving a CE of 62% that rapidly increases to 94% after 10 cycles. The full-cell delivered a reversible capacity of 84 mAh g^{-1} after 50 cycles. Moreover, as shown in Figure 6E, the full-cell capacity of 54 mAh g^{-1} is retained after 1000 cycles at 0.5 A g^{-1}. Rate performance of the full-cell is displayed in Figure 6D, where capacities of 73, 58, and 43 mAh g^{-1} were obtained at the current densities of 0.2 A g^{-1}, 0.5 A g^{-1}, and 1.0 A g^{-1}, respectively. The result is among the best ones of KICs in terms of energy density and power density (Figure S15). [17, 20-27, 29]

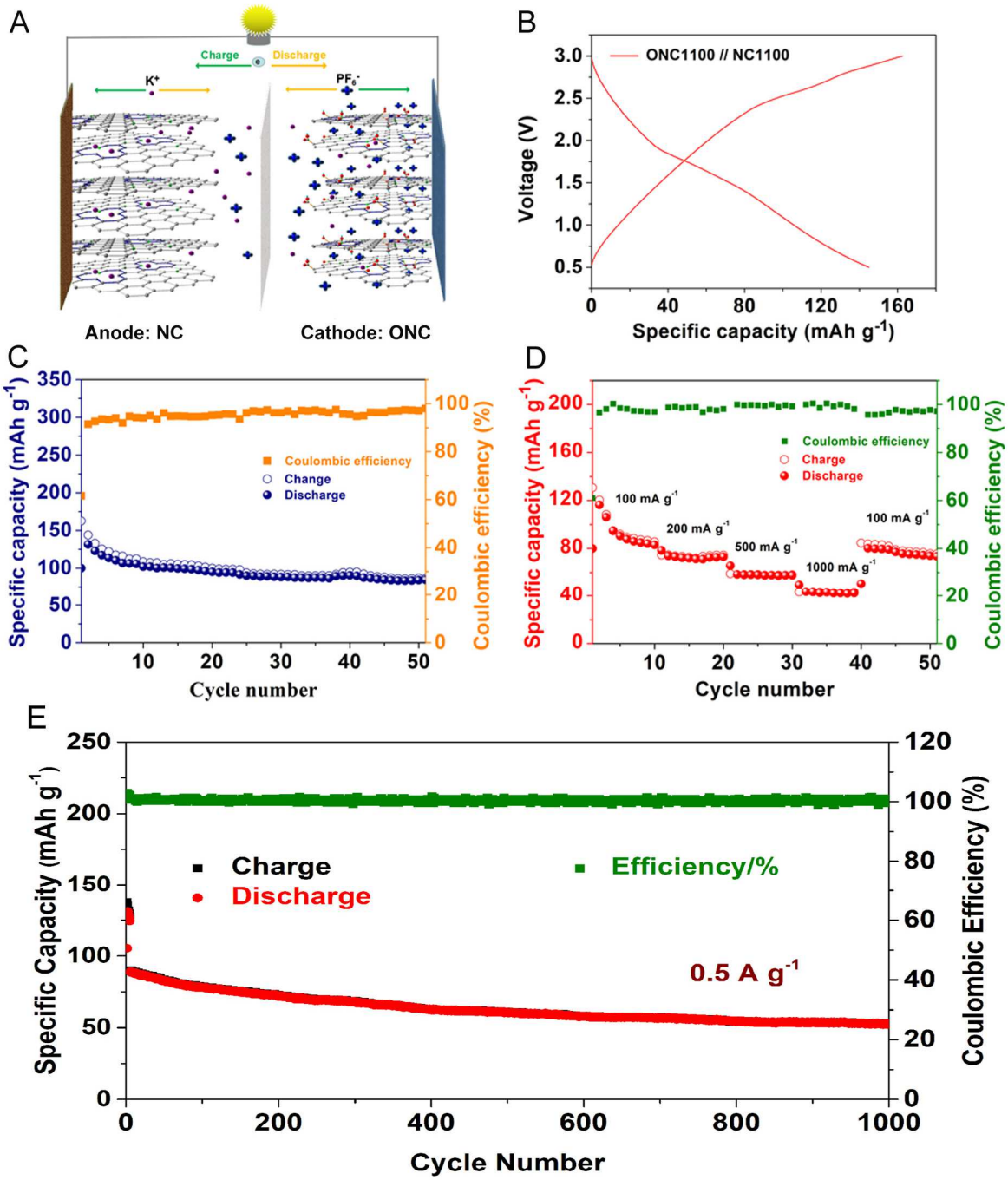

Figure 6. Electrochemical performances of the ONC//NC full cell. (A) Schematic illustration of the charge and discharge processes in full cell. (B) The first charge and second discharge profiles. (C) Cycling performance at the current density 100 mA g^{-1}. (D) Rate performance with various rates ranging from 100 mA g-1 to 1000 mA g^{-1}. (E) The long cycling performance of the

ONC//NC full-cell at 0.5 A g^{-1}.

4. Conclusion

Benefiting from the surface-controlled reaction, oxygen functionalized carbon nanofibers cathode exhibited a large capacity and great rate capability within a high voltage window for K-ion storage. The charge storage mechanism and rational material design highlight an important key element of storing large-sized ions. Surface faradic reaction dominated process instead of diffusion faradic reaction dominated process, which leads to the optimal performance of the promising KICs. We also found out a clue that a soft carbon precursor with suitable graphitization and defects would be a better choice for obtaining stable and oxygen-rich carbon in strong acid. Based on the oxygen functionalization enabled charge storage, we demonstrated an advanced K-ion based full cell consisting of both carbonaceous cathode and anode deriving from a single carbon source. This work may shed light on designing high-performance KIC cathodes and open up an avenue towards future energy storage technologies with low cost and material sustainability.

Appendix A. Supplementary

Low-magnification and high-magnification SEM images of NC and ONC, HRTEM image of NC, electrochemical investigation of NC, C 1s core level of XPS spectra of ONC during different charge/discharge processes, etc.

Author Contributions

C.L.Z and Y. X. contributed equally to this work. Conceptualization, C.L.Z., Y.X., and Y.L.; Methodology, C.L.Z.; Investigation, C.L.Z., G.Y.D., Y.H.W., Y.G.F, Y.L.L., and U.K.; Writing – Original Draft, C.L.Z. Writing – Review & Editing Y.L.; Funding Acquisition, Y.L.; Resources, H.P.Z., and M.Z.; Supervision, Y.L.

Notes

The authors declare no competing financial interest.

Acknowledgements

This work was financially supported by the German Research Foundation (DFG: LE2249/5-1) and National Natural Science Foundation of China (21577086). Additionally, Chenglin Zhang is sponsored by the China Scholarship Council.

References

[1] J. C. Pramudita, D. Sehrawat, D. Goonetilleke, N. Sharma, Adv. Energy Mater. 7 (2017) 1602911.

[2] A. Eftekhari, Z. Jian, X. Ji, ACS Appl. Mater. Interfaces 9 (2017) 4404-4419.

[3] H. Kim, J. C. Kim, M. Bianchini, D.-H. Seo, J. Rodriguez-Garcia, G. Ceder, Adv. Energy Mater. 8 (2018) 1702384.

[4] X. Wu, D. P. Leonard, X. Ji, Chem. Mater. 29 (2017) 5031-5042.

[5] Y. Xie, Y. Chen, L. Liu, P. Tao, M. Fan, N. Xu, X. Shen, C. Yan, Adv. Mater. 29 (2017) 1702268.

[6] W. Wang, J. Zhou, Z. Wang, L. Zhao, P. Li, Y. Yang, C. Yang, H. Huang, S. Guo, Adv. Energy Mater. 8 (2018) 1701648.

[7] C. Chen, Z. Wang, B. Zhang, L. Miao, J. Cai, L. Peng, Y. Huang, J. Jiang, Y. Huang, L. Zhang, J. Xie, Energy Storage Mater. 8 (2017) 161-168.

[8] K. Lei, F. Li, C. Mu, J. Wang, Q. Zhao, C. Chen, J. Chen, Energy Environ. Sci. 10 (2017)

552-557.

[9] H. Kim, J. C. Kim, S.-H. Bo, T. Shi, D.-H. Kwon, G. Ceder, Adv. Energy Mater. 7 (2017) 1700098.

[10] X. Wang, X. Xu, C. Niu, J. Meng, M. Huang, X. Liu, Z. Liu, L. Mai, Nano Lett. 17 (2017) 544-550.

[11] W. B. Park, S. C. Han, C. Park, S. U. Hong, U. Han, S. P. Singh, Y. H. Jung, D. Ahn, K.-S. Sohn, M. Pyo, Adv. Energy Mater. 8 (2018) 1703099.

[12] M. Clites, J. L. Hart, M. L. Taheri, E. Pomerantseva, ACS Energy Lett. 3 (2018) 562-567.

[13] Y.-H. Zhu, X. Yang, D. Bao, X.-F. Bie, T. Sun, S. Wang, Y.-S. Jiang, X.-B. Zhang, J.-M. Yan, Q. Jiang, Joule 2 (2018) 736-746.

[14] L. Xue, Y. Li, H. Gao, W. Zhou, X. Lu, W. Kaveevivitchai, A. Manthiram, J. B. Goodenough, J. Am. Chem. Soc. 139 (2017) 2164-2167.

[15] T. Deng, X. Fan, J. Chen, L. Chen, C. Luo, X. Zhou, J. Yang, S. Zheng, C. Wang, Adv. Funct. Mater. 28 (2018) 1800219.

[16] C. Zhang, Y. Xu, M. Zhou, L. Liang, H. Dong, M. Wu, Y. Yang, Y. Lei, Adv. Funct. Mater. 27 (2017) 1604307.

[17] L. Fan, K. Lin, J. Wang, R. Ma, B. Lu, Adv. Mater. 30 (2018) 1800804.

[18] Z. Zhang, M. Li, Y. Gao, Z. Wei, M. Zhang, C. Wang, Y. Zeng, B. Zou, G. Chen, F. Du, Adv. Funct. Mater. 28 (2018) 1802684.

[19] S. Dong, Z. Li, Z. Xing, X. Wu, X. Ji, X. Zhang, ACS Appl. Mater. Interfaces 10 (2018) 15542-15547.

[20] Y. Luo, L. Liu, K. Lei, J. Shi, G. Xu, F. Li, J. Chen, Chem. Sci. 10 (2019) 2048-2052.

[21] Y. Yi, Z. Sun, C. Li, Z. Tian, C. Lu, Y. Shao, J. Li, J. Sun, Z. Liu, Adv. Funct. Mater. 30 (2019) 1903878.

[22] J. Chen, B. Yang, H. Hou, H. Li, L. Liu, L. Zhang, X. Yan, Adv. Energy Mater. 9 (2019) 1803894.

[23] F. Ming, H. Liang, W. Zhang, J. Ming, Y. Lei, A.-H. Emwas, H.N. Alshareef, Nano Energy 62 (2019) 853-860.

[24] Y. Wang, Z. Zhang, G. Wang, X. Yang, Y. Sui, F. Du, B. Zou, Nanoscale Horiz. 4 (2019) 1394-1401.

[25] J. Chen, B. Yang, H. Li, P. Ma, J. Lang, X. Yan, J. Mater. Chem. A 7 (2019) 9247-9252.

[26] J. Ge, B. Wang, J. Wang, Q. Zhang, B. Lu, Adv. Energy Mater. 10 (2019) 1903277.

[27] H.V. Ramasamy, B. Senthilkumar, P. Barpanda, Y.-S. Lee, Chem. Eng. J. 368 (2019) 235-243.

[28] B. Yang, J. Chen, L. Liu, P. Ma, B. Liu, J. Lang, Y. Tang, X. Yan, Energy Storage Mater. 23 (2019) 522-529.

[29] Z. Xu, M. Wu, Z. Chen, C. Chen, J. Yang, T. Feng, E. Paek, D. Mitlin, Adv. Sci. 6 (2019) 1802272.

[30] Q. Zhao, J. Wang, Y. Lu, Y. Li, G. Liang, J. Chen, Angew. Chem. Int. Ed. 55 (2016) 12528-32.

[31] Z. Jian, Y. Liang, I. A. Rodríguez-Pérez, Y. Yao, X. Ji, Electrochem. Commun. 71 (2016) 5-8.

[32] U. N. Maiti, W. J. Lee, J. M. Lee, Y. Oh, J. Y. Kim, J. E. Kim, J. Shim, T. H. Han, S. O. Kim, Adv. Mater. 26 (2014) 40-66.

[33] Y. Xu, C. Zhang, M. Zhou, Q. Fu, C. Zhao, M. Wu, Y. Lei, Nat. Commun. 9 (2018) 1720.

[34] L. Fan, K. Lin, J. Wang, R. Ma, B. Lu, Adv. Mater. 30 (2018) 1800804.

[35] B. Ji, F. Zhang, N. Wu, Y. Tang, Adv. Energy Mater. 7 (2017) 1700920.

[36] L. Fan, Q. Liu, S. Chen, K. Lin, Z. Xu, B. Lu, Small 13 (2017) 1701011.

[37] K. Beltrop, S. Beuker, A. Heckmann, M. Winter, T. Placke, Energy Environ. Sci. 10 (2017) 2090-2094.

[38] Y. Wen, K. He, Y. Zhu, F. Han, Y. Xu, I. Matsuda, Y. Ishii, J. Cumings, C. Wang, Nat. Commun. 5 (2014) 4033.

[39] J. Ding, H. Wang, Z. Li, K. Cui, D. Karpuzov, X. Tan, A. Kohandehghan, D. Mitlin, Energy Environ. Sci. 8 (2015) 941-955.

[40] T. Van Khai, H. G. Na, D. S. Kwak, Y. J. Kwon, H. Ham, K. B. Shim, H. W. Kim, J. Mater. Chem. 22 (2012) 17992.

[41] M. Acik, C. Mattevi, C. Gong, G. Lee, K. Cho, M. Chhowalla, Y. J. Chabal, ACS Nano 4 (10) 5861-5868.

[42] S. W. Lee, N. Yabuuchi, B. M. Gallant, S. Chen, B. S. Kim, P. T. Hammond, Y. Shao-Horn, Nat. Nanotechnol. 5 (2010) 531-537.

[43] S. W. Lee, B.-S. Kim, S. Chen, Y. Shao-Horn, P. T. Hammond, J. Am. Chem. Soc. 131 (2009) 671-679.

[44] J. Liao, Q. Hu, Y. Yu, H. Wang, Z. Tang, Z. Wen, C. Chen, J. Mater. Chem. A 5 (2017) 19017-19024.

[45] J. Ma, E. Zhou, C. Fan, B. Wu, C. Li, Z. H. Lu, J. Li, Chem. Commun. 54 (2018) 5578-5581.

[46] Z. Shadike, D.-R. Shi, T.-W. Tian-Wang, M.-H. Cao, S.-F. Yang, J. Chen, Z.-W. Fu, J. Mater. Chem. A 5 (2017) 6393-6398.

[47] J. Zheng, W. Deng, Z. Hu, Z. Zhuo, F. Liu, H. Chen, Y. Lin, W. Yang, K. Amine, R. Li, J. Lu, F. Pan, ACS Energy Lett. 3 (2017) 65-71.

[48] H. Kim, Y.-U. Park, K.-Y. Park, H.-D. Lim, J. Hong, K. Kang, Nano Energy 4 (2014) 97-104.

[49] S. Chen, J. Wang, L. Fan, R. Ma, E. Zhang, Q. Liu, B. Lu, Adv. Energy Mater. 8 (2018) 1800140.

[50] Y. Xu, M. Zhou, Y. Lei, Mater. Today 21 (2018) 60-78.

[51] Q. Zhao, Y. Lu, J. Chen, Adv. Energy Mater. 7 (2017) 1601792.

[52] M. Armand, S. Grugeon, H. Vezin, S. Laruelle, P. Ribiere, P. Poizot, J.M. Tarascon, Nat. Mater. 8 (2009) 120-125.

[53] Q. Deng, J. Pei, C. Fan, J. Ma, B. Cao, C. Li, Y. Jin, L. Wang, J. Li, Nano Energy 33 (2017) 350-355.

[54] V. Augustyn, J. Come, M. A. Lowe, J. W. Kim, P. L. Taberna, S. H. Tolbert, H. D. Abruna, P. Simon, B. Dunn, Nat. Mater. 12 (2013) 518-22.

[55] S. Ardizzone, G. Fregonara, S. Trasatti, Electrochim. Acta 35 (1989) 263-267.

- The carbon nanofibers with high-content -C=O groups was obtained by an efficient oxygen functionalization engineering.
- The carbon nanofibers exhibited great capability of potassium-ion storage within a high voltage window of 1.2 - 4.2 V.
- Surface-dominated reaction of -C=O + K^+ + e $\leftrightarrow$ -C-O-K was verified as the major contributor for the enhancement of potassium-ion storage.
- A “green” potassium-ion hybrid capacitor with both carbon cathode and anode that are derived from same precursor was demonstrated.

Declaration of interests

☒ The authors declare that they have no known competing financial interests or personal relationships that could have appeared to influence the work reported in this paper.

☐The authors declare the following financial interests/personal relationships which may be considered as potential competing interests: